Observation of the *L-H* Confinement Bifurcation Triggered by a Turbulence-Driven Shear Flow in a Tokamak Plasma

Z. Yan,[1,*] G. R. McKee,[1] R. Fonck,[1] P. Gohil,[2] R. J. Groebner,[2] and T. H. Osborne[2]
[1]*University of Wisconsin-Madison, Madison, Wisconsin 53706, USA*
[2]*General Atomics, PO Box 85608, San Diego, California 92186-9784, USA*
(Received 26 June 2013; published 24 March 2014)

Comprehensive 2D turbulence and eddy flow velocity measurements on DIII-D demonstrate a rapidly increasing turbulence-driven shear flow that develops ~100 μs prior to the low-confinement (L mode) to high-confinement (H mode) transition and appears to trigger it. These changes are localized to a narrow layer 1–2 cm inside the magnetic boundary. Increasing heating power increases the Reynolds stress, the energy transfer from turbulence to the poloidal flow, and the edge flow shearing rate that then exceeds the decorrelation rate, suppressing turbulence and triggering the transition.

DOI: 10.1103/PhysRevLett.112.125002 PACS numbers: 52.55.−s, 52.30.−q, 52.35.Ra

Magnetically confined plasmas undergo an as yet unexplained transition from a low-confinement state (L mode) to a high-confinement state (H mode) as the heating power across the boundary surface exceeds a specific threshold [1]. The resulting H-mode state achieves a substantially higher global energy confinement time and plasma pressure (β), and is thus envisioned as the operating mode of choice for future burning plasma experiments and ultimately fusion reactors [2]. This bifurcation from L to H mode (L-H transition) is characterized by a rapid suppression of turbulence at the plasma edge, reduced D_α recycling light emission, buildup of a sharp edge pressure pedestal, formation of an E_r well, increased $E \times B$ shearing rate, and formation of a particle and energy transport barrier. The importance of this transport barrier is not limited to magnetically confined plasmas but has also been widely recognized in other fluid systems, especially those that are dominantly 2D in nature, such as geophysical and atmospheric fluid systems, etc. [3,4]. Numerous theoretical models have been developed to explain the L-H transition and its dependence on plasma parameters [5]. The mathematical concept of bifurcation theory was applied to L-H transitions to distinguish systems that undergo sharp transitions or oscillatory limit-cycle transitions [6].

The precise triggering event that causes the transition in plasmas has been predicted to approximately depend on the relationship of edge turbulence properties and $E \times B$ flow shear, the so called predator-prey model [7]. In this model, increasing heat flux across the edge of the plasma results in stronger turbulence (prey). The growing turbulence will nonlinearly drive shear flow (predator) through Reynolds stress. When the drive is larger than the flow damping, a poloidal flow will grow and extract kinetic energy from the turbulence and, hence, suppress turbulence and the associated turbulent transport. As a result, the mean radial electric field shear increases to a value that can maintain the suppression of turbulence and the H mode. Recently, the limit-cycle-oscillation has been observed with the characteristics of a predator-prey system during the low-intermediate-high confinement (L-I-H) transition in various machines [8–13]. However, the L-H transition more typically occurs directly without the intermediate phase oscillations.

One recent theory predicted that a direct L-H transition can be triggered by a single burst of axisymmetric radially sheared flow (known as zonal flow [14]) energy that extracts most or all of the energy from the turbulence [15]. Previous experiments demonstrated generation of poloidal shear flow via Reynolds stress [16] and the apparent role of changing turbulence mode structure and increased low-frequency poloidal flows and flow shear in causing the L-H transition [17]. An experiment on Experimental Advanced Superconducting Tokamak (EAST) has demonstrated clear evidence of a zonal flow triggering an L-H transition with probe measurements [18]. There have been no reports on both temporally and spatially resolved behavior of turbulence and flow during a direct L-H transition. In addition, there have been no previous reports on visualization of the turbulent eddy dynamics during this process.

This Letter reports the first comprehensive 2D experimental investigation of the rapidly increasing shear flow generated from turbulence prior to and triggering the L-H transition with beam emission spectroscopy (BES) measuring the spatiotemporal density fluctuations and the derived flows. These measurements reveal the critical role of turbulence kinetic energy transfer between plasma turbulence and poloidal velocity flows in triggering the L-H transition, as well as the detailed time-resolved evolution of turbulence, turbulence-driven sheared flows, and inferred Reynolds stress that take place during the critical time interval leading up to the transition. This time-resolved process is visualized via 2D imaging of the turbulence dynamics (see the Supplemental Material [19]).

The experiment was carried out on the DIII-D tokamak with a lower-single-null plasma shape with the ion ∇B drift

towards the X point ($B_T = 2$ T, $I_p = 1$ MA), with neutral beams injected tangentially in the direction of the plasma current. Long wavelength ($k_\perp \rho_i < 1$), localized density fluctuations are measured with BES, which measures Doppler-shifted D_α emission from collisionally excited high-energy neutral beam atoms. The light intensity is related to the local density through the atomic physics of beam atom excitation [20]. An 8×8 2D array of BES channels, each channel imaging a $0.9\,\mathrm{cm}\,(\mathrm{radial}) \times 1.2\,\mathrm{cm}\,(\mathrm{poloidal})$ area is located at the plasma edge ($0.88 < \psi < 1+$), providing fully two-dimensional measurements of the turbulence dynamics [21].

Figure 1(a) illustrates major features of the L-H transition with a time series of neutral beam injection power, D_α emission, and line-averaged electron density. The L-H transition occurs at $t \sim 1558$ ms and is indicated by the sudden drop in the D_α signal. In this work, the dynamics of turbulence and flow are investigated by comparing their behaviors at two different power levels leading to the transition: one at lower input power ($P < P_{LH}$), and the second just before the transition ($P > P_{LH}$, where P_{LH} is the power threshold for the transition). Each time window used in the analysis is 10 ms. Figure 1(b) shows a radial profile of the density fluctuation amplitudes as a function of ψ (normalized poloidal flux) from BES measurements integrated over 20 to 150 kHz, where broadband turbulence is observed, averaged over these two time windows. It shows that the density fluctuation amplitudes increase with heating power. The poloidal and radial correlation length of these fluctuations is about 2.5–3.5 cm and 1.5 cm, respectively. These are both larger than the BES system spot size and allow for the low-wave-number density fluctuation spectrum to be well resolved.

With the capability of 2D turbulence measurements, nearly instantaneous poloidal and radial velocity field measurements $\tilde{V}_r$ and $\tilde{V}_\theta$ can be obtained by applying a velocimetry technique [22] to the density fluctuation imaging. The coherence level between $\tilde{V}_r$ and $\tilde{V}_\theta$ is well above the noise level. This technique has been reported and tested previously [23]. The density fluctuations were first frequency filtered over the range 20 to 150 kHz. With these measured fluctuating radial and poloidal velocities, the inferred Reynolds stress RS can be calculated as $\mathrm{RS} = \langle \tilde{V}_r \tilde{V}_\theta \rangle$. The application of this technique and the derived velocity dynamics have been compared with the Langmuir probe measurements during the limit-cycle-oscillation experiments, which provide reasonably good agreement [13]. This technique has the merit of obtaining the velocity field at the sampling time for BES (1 μs) to capture the fast flow dynamics. By comparison, the turbulence decorrelation time or eddy lifetime for this low-wave-number turbulence is of order several microseconds.

A detailed time series of the normalized density fluctuations, inferred Reynolds stress gradient, poloidal velocity, and shearing rate at an early time at lower input power ($P < P_{LH}$) is shown in Fig. 2 in black. The density fluctuations are frequency filtered from 40 to 60 kHz where the fluctuation energy peaks, and the turbulent velocity fields and Reynolds stress are computed as described above. The poloidal velocity shearing rate is taken as the gradient of the radially adjacent velocity fields, i.e., two radially separated BES channels ($\Delta r \approx 0.9$ cm). These quantities are smoothed over a 50 μs time window. The light gray (blue) horizontal bar in panel (v) of Fig. 2(a) is the turbulence decorrelation rate γ_{decorr}, which is $1/\tau_c$,

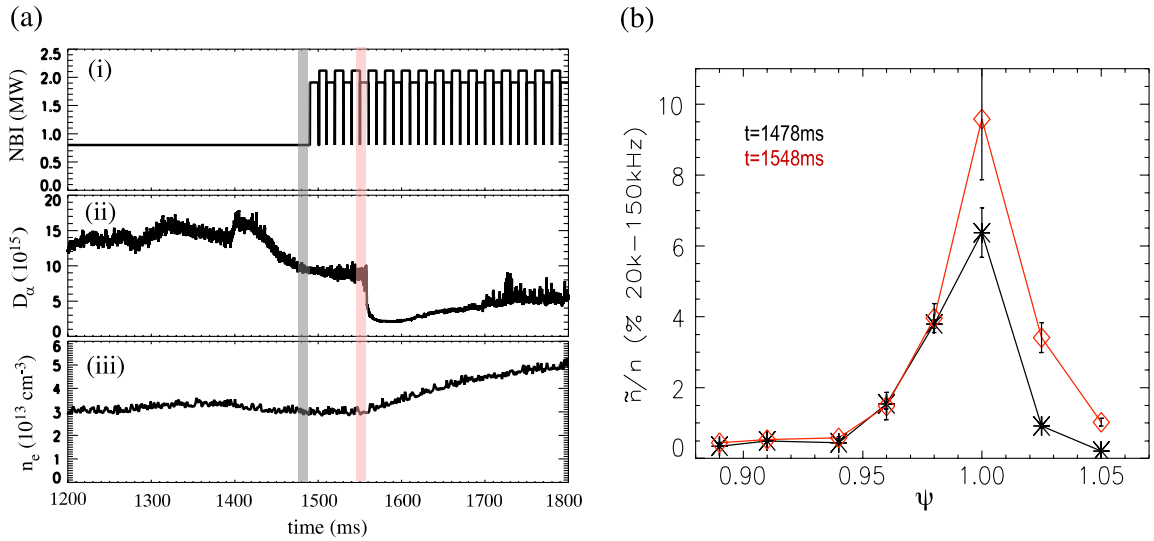

FIG. 1 (color online). (a) Time series of (i) neutral beam injection power, (ii) D_α emission, and (iii) line-averaged electron density. Gray and light gray (red) shades indicate the two time windows analyzed in the Letter. (b) Radial profile of relative density fluctuation amplitudes frequency integrated from 20 to 150 kHz; black is for lower heating power ($t = 1478$–1488 ms) and light gray (red) is for higher heating power just before the transition ($t = 1548$–1558 ms).

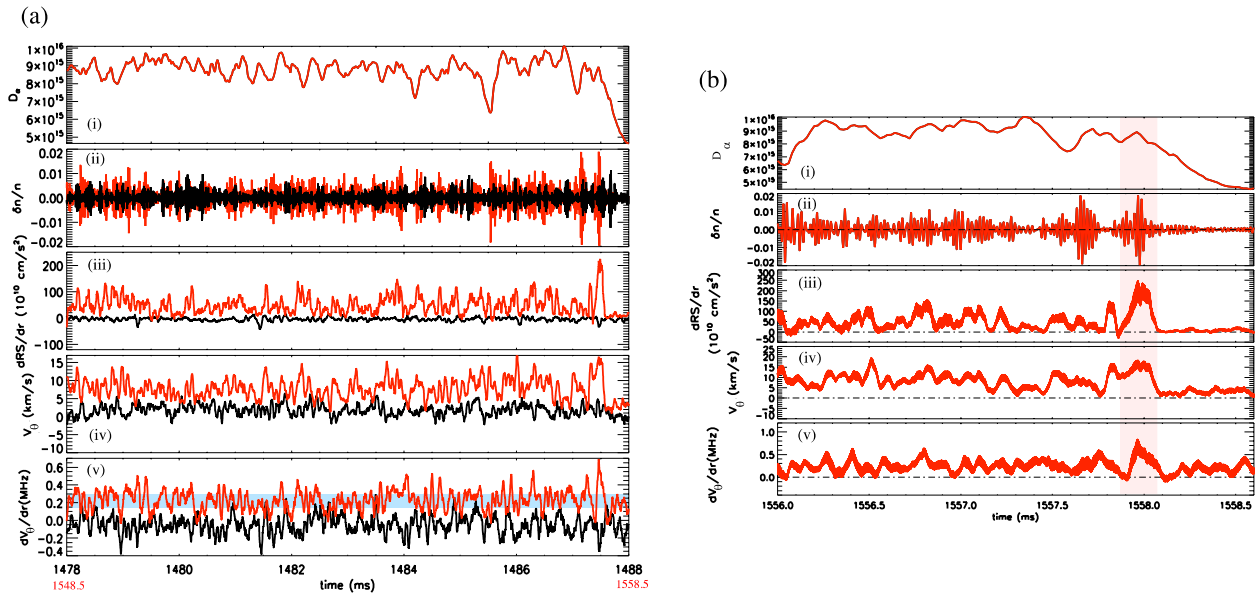

FIG. 2 (color online). (a) Time series of (i) D_α emission, (ii) relative density fluctuation amplitude, (iii) Reynolds stress gradient, (iv) poloidal velocity, and (v) poloidal velocity shearing rate. Black is for early time about 80 ms before the L-H transition when heating power is lower ($P < P_{LH}$) ($t = 1478$–1488 ms) and gray (red) is for the time 10 ms before and across the transition ($t = 1548.5$–1558.5 ms) and higher power ($P > P_{LH}$). This is at radial position $\psi \sim 0.98$. (b) Zoom in of the last 2 ms time window of the data. The line thickness is the systematic error bar.

measured with BES. τ_c is determined from multiple poloidally separated measurements, and is defined as the inverse of the e-folding time of the decay in peak amplitude of the time-delay cross correlation function between the poloidally displaced BES channels [24]; it is measured in the plasma frame and thus not dependent on the plasma frame velocity. It is estimated over the 10 ms time window in which the turbulence amplitude is approximately time stationary. This decorrelation rate indicates the rate of energy transfer to the higher wave number region where viscous dissipation occurs. It is found that the turbulence decorrelation rate on average exceeds the poloidal flow-shearing rate at this early time when $P < P_{LH}$. To compare to the later time immediately prior to the transition ($P > P_{LH}$), the same quantities are over plotted on the same scale in Fig. 2(a) [shown in gray (red)]. The turbulence amplitude, Reynolds stress gradient, and shearing rate all increase significantly compared to the early time (black traces) before the input power is increased. The shearing rate now becomes comparable to or exceeds the decorrelation rate as the transition is approached.

Of particular interest is the dynamics immediately before the transition (~100 μs): a rapid increase in the turbulence amplitude, Reynolds stress gradient, and poloidal flow are simultaneously observed as shown in Fig. 2(b), which zooms in on the last 2 ms across the L-H transition. The line thickness indicates the systematic error bar estimated from a standard deviation of the mean over eight poloidal channel measurements. Immediately before the transition, the Reynolds stress gradient, poloidal flow, and shear all sharply increase. After this final burst, the plasma enters H mode, and turbulence is suppressed. This last rapid increase of the flow drive from the inferred Reynolds stress gradient [Fig. 3(a)] and the poloidal flow shearing rate [Fig. 3(b)] is highly localized to the region 1–2 cm inside the separatrix as determined by magnetic equilibrium reconstruction via EFIT. No such evolution of these turbulence quantities is observed further inside the plasma or outside on the open field line (scrape-off layer) region. These observations suggest that the burst of the sheared flow is generated by the burst of turbulence that then triggers the L-H transition.

Further evidence of the turbulence driven shear flow comes from the investigation of the nonlinear energy

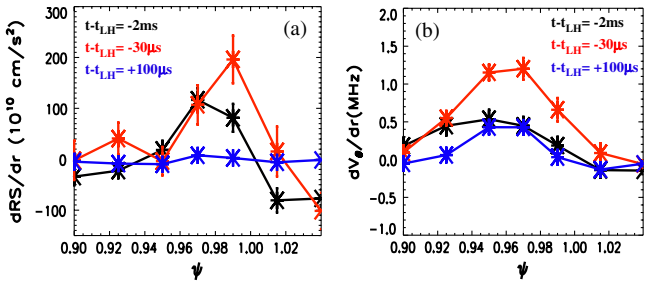

FIG. 3 (color online). Radial profile of (a) Reynolds stress gradient and (b) poloidal velocity shearing rate. Black is at a time about 2 ms before the transition, light gray (red) is at the time just before the transition and dark gray (blue) is at the time after the transition. The L-H transition is at 1558 ms.

transfer. This process should take place at the same time and spatial position where the bursts of turbulence and shear flow are observed. In the predator-prey model [7], we can write the evolution for both zonal flow and turbulence as in Ref. [18],

$$\frac{\partial \tilde{V}_\perp^2}{\partial t} = \gamma_{\rm eff}\tilde{V}_\perp^2 - \langle \tilde{V}_r \tilde{V}_\theta \rangle \frac{\partial V_{\rm ZF}}{\partial r},$$
$$\frac{\partial V_{\rm ZF}^2}{\partial t} = \langle \tilde{V}_r \tilde{V}_\theta \rangle \frac{\partial V_{\rm ZF}}{\partial r} - \mu V_{\rm ZF}^2. \quad (1)$$

Here, $\gamma_{\rm eff}$ is the total effective growth rate of turbulence, μ is the total zonal flow damping rate, including collisional, charge exchange, and nonlinear damping, $\tilde{V}_\perp^2 = \tilde{V}_r^2 + \tilde{V}_\theta^2$ is the perpendicular turbulence kinetic energy, $V_{\rm ZF}$ is the zonal flow velocity, and $P_\perp = \langle \tilde{V}_r \tilde{V}_\theta \rangle (\partial V_{\rm ZF}/\partial r)$ is the Reynolds power generated by the fluctuations on the flow per unit mass. Energy input into the turbulence from the gradients of n_e, T_e, etc., is balanced by transfer to both smaller scales where the turbulence is dissipated by viscosity as well as to larger scales that drive the poloidal zonal flow. $P_\perp$ can be calculated in the time domain using suitably filtered and averaged quantities from the BES measurements [25,26]. This term acts like an energy source for the shear flow. It is a transfer channel between the turbulent energy and the flow energy with different signs in Eq. (1), appearing as a sink in the first equation, and a source in the second equation. Therefore, the generation process of zonal flows directly includes a suppression mechanism of the turbulence by extracting energy from the turbulence, and so when $(\langle \tilde{V}_r \tilde{V}_\theta \rangle (\partial V_{\rm ZF}/\partial r)/\gamma_{\rm eff}\tilde{V}_\perp^2) > 1$, $(\partial \tilde{V}_\perp^2/\partial t) < 0$ and turbulence is suppressed.

Figure 4 shows the time series of the rate of energy transfer $P_\perp/\tilde{V}_\perp^2$ in the same time window as Fig. 2(b) at three different radial locations. The black line is near the gradient of the pedestal region, and the light gray (red) and dark gray (blue) lines are further inside the plasma. It is found that immediately before the L-H transition at 1558 ms, the energy transfer between turbulence and shear flow increases rapidly at the same time as the increase of shear flow (seen in Fig. 2) and is localized to the same pedestal region where the turbulence and shear flow rapidly develop (Fig. 3). $P_\perp/\tilde{V}_\perp^2$ is generally positive near the pedestal gradient region, which suggests that at this location the energy is on average transferred from turbulence to the shear flow. A comparison of $P_\perp/\tilde{V}_\perp^2$ with the plasma frame turbulent decorrelation rate $\gamma_{\rm decorr}$ [shown in panel (v) of Fig. 2(a) as the light gray (blue) bar] [13] finds that these quantities are comparable before the final increase of energy transfer, ~ 2–3×10^5 s^{-1}, suggesting energy is equally transferred into two scales. We can estimate the effective turbulence recovery rate $\gamma_{\rm eff} \approx \gamma_{\rm decorr} + P_\perp/\tilde{V}_\perp^2 \approx 4$–$6 \times 10^5$ s^{-1} given that the L-mode state is time stationary during the time window on the order of 1 ms. Immediately prior to the L-H transition, the energy transfer rate increases by 2–3 times and exceeds the net energy input rate into the turbulence $\gamma_{\rm eff} - \gamma_{\rm decorr}$. As a result, turbulence is quenched and the system is driven into H mode.

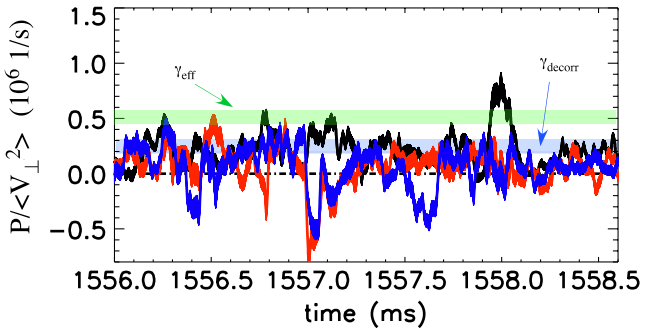

FIG. 4 (color online). Time series of normalized energy production into the flow, $P_\perp/\langle \tilde{V}_\perp^2 \rangle = \langle \tilde{V}_r \tilde{V}_\theta \rangle (\partial V_{\rm ZF}/\partial r)/\langle \tilde{V}_\perp^2 \rangle$. Black is at $\psi \sim 0.98$, light gray (red) is at $\psi \sim 0.96$, and dark gray (blue) is at $\psi \sim 0.93$. The line thickness is the systematic error bar.

This turbulence suppression process can be directly visualized with density fluctuation images from BES (see the Supplemental Material [19]). Shown in Fig. 5 is a sequence of turbulence images taken at the time just before the L-H transition with a time difference of 2 μs between each frame. The solid black line represents the separatrix. The images are generated by frequency filtering the density fluctuation data from 20 to 150 kHz and performing a spline fit to the spatial data. Light gray (red) [dark gray (blue)] represents positive (negative) density perturbation amplitudes. The arrows on the images indicate the instantaneous velocity field derived via velocimetry. Turbulent eddies propagate downwards just inside

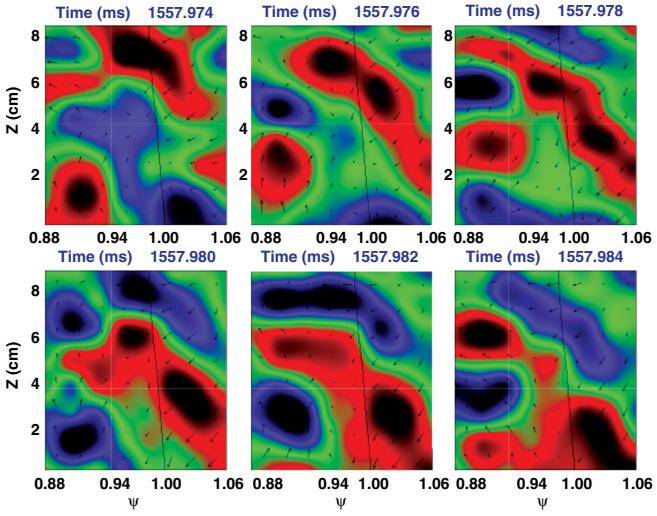

FIG. 5 (color online). A set of 2D density fluctuation images from BES at consecutive times with $\Delta t = 2$ μs. The solid black line represents the separatrix. The calculated inferred velocity field is superimposed as black arrows; light gray (dark gray) [red (blue)] refers to positive (negative) density fluctuations, with whitish (green) the equilibrium density.

the separatrix, which is in the electron diamagnetic direction in the laboratory frame, while they propagate upwards (ion diamagnetic direction) further inside. In addition, as the turbulent eddies move downward just inside the separatrix, they become tilted by the sheared flow, after which they are suppressed, indicated by the reduction of the amplitudes of the turbulent eddies at the shear layer region. This occurs when and where the increase in nonlinear kinetic energy transfer from turbulence to the flow is observed. It is consistent with observations of fluctuation depletion and eddy splitting seen in the Controlled Shear Decorrelation Experiment (CSDX) using fast visible imaging diagnostics [27]. It will be interesting to investigate the statistical properties of the turbulent eddies across the L-H transition [28] with these measurements. A full specific paper regarding this is in process and will be reported in the future. We also note that an ultrafast charge exchange recombination spectroscopy (UF-CHERS) system [29] is under development, which will provide fast ion temperature profile measurements in future experiments.

In conclusion, the measured spatiotemporal behavior of the turbulence and flows prior to the transition indicate that a transient increase in poloidally sheared flow and turbulent stress plays the critical role in triggering the L-H transition. The experimental data demonstrate that the increased heat flux leads to increased turbulent drive for the shear flow at the edge of the plasma through nonlinear energy transfer prior to the L-H transition. When the rate of energy transfer into the shear flow exceeds the power input into the turbulence, the turbulence amplitude collapses. The turbulent transport then drops, resulting in an increase in the edge pressure gradient. The radial electric field then grows just inside the separatrix, sustaining turbulence suppression, as the system is driven into H mode. These observations reported here for one plasma have been obtained in multiple discharges under similar plasma conditions, as well as at a lower toroidal field (the toroidal field dependence of the L-H transition dynamics will be addressed in a subsequent publication). These results provide critical new information demonstrating the L-H dynamics and build on a substantial body of evidence that turbulence-driven zonal flows play an important role in triggering the L-H transition [8–13,16–18,30]. This Letter reports the first 2D evidence of the fast turbulence and flow response arising from energy transfer in a conventional fast L-H transition.

This work is supported by the U.S. Department of Energy under Grants No. DE-FG02-89ER53296, No. DE-FG02-08ER54999, No. DE-FC02-04ER54698, and No. DE-FG02-95ER54309. The authors appreciate the support of the DIII-D team for these experiments and valuable discussions with G. R. Tynan and P. H. Diamond, and interactions with the CMTFO center (University of California, San Diego).

*Corresponding author.
zyan5@wisc.edu

[1] F. Wagner, Plasma Phys. Controlled Fusion **49**, B1 (2007).
[2] C. Gormezano *et al.*, Nucl. Fusion **47**, S285 (2007).
[3] C. R. Or and F. H. Busse, J. Fluid Mech. **174**, 313 (1987).
[4] M. E. McIntyre, J. Atmos. Terr. Phys. **51**, 29 (1989).
[5] J. W. Connor and H. R. Wilson, Plasma Phys. Controlled Fusion **42**, R1 (2000).
[6] W. Weymiens, H. J. de Blank, G. M. D. Hogeweij, and J. C. de Valença, Phys. Plasmas, **19**, 072309 (2012).
[7] E. J. Kim and P. H. Diamond, Phys. Rev. Lett. **90**, 185006 (2003).
[8] G. D. Conway, C. Angioni, F. Ryter, P. Sauter, and J. Vicente, Phys. Rev. Lett. **106**, 065001 (2011).
[9] T. Estrada, T. Happel, C. Hidalgo, E. Ascasíbar, and E. Blanco, Europhys. Lett. **92**, 35001 (2010).
[10] P. Manz, M. Ramisch, and U. Stroth, Phys. Rev. E **82**, 056403 (2010).
[11] G. S. Xu *et al.*, Phys. Rev. Lett. **107**, 125001 (2011).
[12] L. Schmitz, L. Zeng, T. L. Rhodes, J. C. Hillesheim, E. J. Doyle, R. J. Groebner, W. A. Peebles, K. H. Burrell, and G. Wang, Phys. Rev. Lett. **108**, 155002 (2012).
[13] G. R. Tynan *et al.*, Nucl. Fusion, **53**, 073053 (2013).
[14] P. Diamond, S.-I. Itoh, K. Itoh, and T. S. Hahm, Plasma Phys. Controlled Fusion, **47**, R35 (2005).
[15] K. Miki, Phys. Plasmas **19**, 092306, (2012).
[16] C. Hildalgo *et al.*, Plasma Phys. Controlled Fusion, **42**, A153, (2000).
[17] G. R. McKee *et al.*, Nucl. Fusion **49**, 115016 (2009).
[18] P. Manz *et al.*, Phys. Plasmas, **19**, 072311, (2012).
[19] See Supplemental Material at http://link.aps.org/supplemental/10.1103/PhysRevLett.112.125002 for a 2D density fluctuation movie measured with BES.
[20] R. Fonck, P. A. Duperrex, and S. F. Paul, Rev. Sci. Instrum. **61**, 3487 (1990).
[21] G. R. McKee, R. J. Fonck, M. W. Shafer, I. U. Uzun-Kaymak, and Z. Yan, Rev. Sci. Instrum. **81**, 10D741 (2010).
[22] G. M. Quénot, J. Pakleza, and T. A. Kowalewski, Exp. Fluids **25**, 177 (1998).
[23] G. R. McKee, R. J. Fonck, D. K. Gupta, D. J. Schlossberg, M. W. Shafer, C. Holland, and G. Tynan, Rev. Sci. Instrum. **75**, 3490 (2004).
[24] G. R. McKee, R. J. Fonck, D. K. Gupta, D. J. Schlossberg, M. W. Shafer, R. L. Boivin, and W. Solomon, Plasma Fusion Res. **2**, S1025 (2007).
[25] E. Sanchez, C. Hidalgo, B. Gonçalves, C. Silva, M. A. Pedrosa, M. Hron, and K. Erents, J. Nucl. Mater. **337-339** 296 (2005).
[26] P. Manz, M. Xu, N. Fedorczak, S. C. Thakur, and G. R. Tynan, Phys. Plasmas **19**, 012309 (2012).
[27] N. Fedorczak, P. Manz, S. Chakraborty Thakur, M. Xu, and G. R. Tynan, Plasma Phys. Controlled Fusion **55**, 025011 (2013).
[28] A. Alonso *et al.*, Plasma Phys. Controlled Fusion **48**, B465 (2006).
[29] I. U. Uzun-Kaymak, R. J. Fonck, and G. R. McKee, Rev. Sci. Instrum. **83**, 10D526 (2012).
[30] Y. H. Xu, C. Yu, J. Luo, J. Mao, B. Liu, J. Li, B. Wan, and Y. Wan, Phys. Rev. Lett. **84**, 3867m(2000).